2015

Simulation Study of HEMT Structures With HfO2 Cap Layer For Mitigating Inverse Piezoelectric Effect Related Device Failures

Deepthi Nagulapally
Old Dominion University

Ravi P. Joshi
Old Dominion University

Aswini Pradhan

Original Publication Citation

Nagulapally, D., Joshi, R. P., & Pradhan, A. (2015). Simulation study of HEMT structures with HfO2 cap layer for mitigating inverse piezoelectric effect related device failures. *AIP Advances, 5*(1), 1-12. doi: 10.1063/1.4905702

Simulation study of HEMT structures with HfO_2 cap layer for mitigating inverse piezoelectric effect related device failures

Deepthi Nagulapally,[1] Ravi P. Joshi,[1,a] and Aswini Pradhan[2]
[1]*Department of Electrical and Computer Engineering, Old Dominion University, Norfolk, VA 23529-0246, USA*
[2]*Department of Engineering and Center for Materials Research, Norfolk State University, 700 Park Avenue, Norfolk, VA 23504, USA*

(Received 18 August 2014; accepted 19 December 2014; published online 7 January 2015)

The Inverse Piezoelectric Effect (IPE) is thought to contribute to possible device failure of GaN High Electron Mobility Transistors (HEMTs). Here we focus on a simulation study to probe the possible mitigation of the IPE by reducing the internal electric fields and related elastic energy through the use of high-*k* materials. Inclusion of a HfO_2 "cap layer" above the AlGaN barrier particularly with a partial mesa structure is shown to have potential advantages. Simulations reveal even greater reductions in the internal electric fields by using "field plates" in concert with high-*k* oxides. [http://dx.doi.org/10.1063/1.4905702]

I. INTRODUCTION

Group III nitride semiconductor materials have shown great potential in many microwave power applications such as wireless communication, radar, and automobile electronics. Its mainstream electronic device structure is the AlGaN/GaN high electron mobility transistor (HEMT) which has undergone intense research for radio frequency (RF) and microwave power amplifier applications, cellular and personal communications services, and widespread broadband access.[1]

Advantages include high breakdown fields that can be sustained in GaN HEMT devices because of the large bandgap of the semiconductor, the high electron densities of the two-dimensional electron gas (2DEG) in the channel due to strong piezoelectric and spontaneous polarization effects,[2] and the high electron drift velocities, that are the foundations for high power electronic applications. Higher electron mobilities due to reduced ionized impurity scattering in HEMT structures is an added benefit. Consequently, HEMTs fabricated from GaN can generate four to five times the amount of power that a comparable GaAs HEMT, or conversely the fabrication of much smaller size devices is possible with the same output power.[3] With a low value of On-Resistance (R_{on}) associated with the polarization effects, the breakdown voltage for GaN materials is almost an order of magnitude higher than that for Si-devices.[4] The low R_{on} coupled with high breakdown voltages (V_{br}) are of paramount importance in power switching applications such as factory automation, telecommunications and motor control.[5]

However, it has experimentally been observed that GaN HEMT devices used for high voltage operation can often fail.[2] While hot electron effects (or perhaps electromigration) may be the usual suspect, it has recently been hypothesized that the AlGaN/GaN device failures studied could arise from defect formation associated with the inverse piezoelectric effect (IPE) when operating under high electric fields.[6–8] The basic source is the piezoelectric nature of the GaN and AlGaN materials that leads to increased strain and eventual degradation causing defects at high internal electric

[a]Corresponding author: Email: rjoshi@odu.edu

fields. Defects can affect the device properties such as the background current levels, the turn-on and turn-off voltage levels, increase intrinsic noise, and lead to current collapse. Current collapse[9–14] reduces the transistor RF output power. Basically, under high voltage conditions in small devices (with reduced size intended to decrease transit time and improve frequency response), the high electric fields introduce strong tensile stress in the AlGaN barrier layer that peaks in regions which are typically below the gate edge on the drain side. The stress increases the stored elastic energy inside the AlGaN, and if this exceeds a critical value (about 0.49 J/m^2 Ref. 7), crystallographic defects are formed that are electrically active. This can provide a path for excess gate leakage current, and result in electron trapping that depletes the sheet charge in the channel resulting in current degradation. The IPE can also cause increases in resistance and a positive shift in threshold voltage. In order to mitigate this degradation mechanism, *one needs to minimize the initial strain in the AlGaN barrier layer, by managing the electric field distribution and especially reducing its peak value under the gate*. Some of the other observable device effects of the IPE, consistent with the hypothesis that stress generates traps, are: (i) increases in drain access-resistance and consequent compression in drain current (I_D) and transconductance (g_m) reductions, (ii) larger gate-lag and related current collapse phenomena,[15,16] and (iii) decrease surface conductance between gate and drain and/or attenuated electron injection by the gate, with the latter resulting in gate current (I_G) decreases.

The IPE differs from the better known Hot Electron Effect (HEF). In the HEF, energetic electrons may be trapped on the device surface, in the AlGaN, or in the buffer. This can give rise to reversible degradation of drain current and the transconductance g_{m}.[17] However, these effects *do not have to be permanent*. Effects associated with the IPE, on the other hand, do not require electron flow, and so significant changes in device electrical parameters can occur during the OFF-state. In the case of hot-electron induced effects, the device may be recoverable, and a series of accelerated testing results would be independent of each other without any cumulative effects. With IPE, on the other hand, cumulative effects are very likely.

Also, at higher temperatures, the electron mean free path (which is dictated by phonon scattering) will be shorter. Hence, a higher electric field (i.e., bias voltage) would be necessary for the hot electrons to gain enough energy to cause degradation. Consequently, at a given voltage, the hot-electron route towards degradation would become more difficult due to heating. However, in the case of the IPE, higher temperatures would make it easier to cause stress and trap formation as these processes are based on processes governed by an activation energy barrier.

An important consideration for reliable AlGaN/GaN HEMT device performance is to reduce the electric-field peak value at the drain side of the gate electrode that can lead to stress and defect formation via the IPE. A possible solution is through the use of metal field plates to shape the potential,[18] an idea originally proposed in the context of silicon planar diodes.[19] The field plate (FP) can reduce the maximum electric field by offering an additional surface for termination of the field lines (effectively spreading the electric field over a longer gate-to-drain spacing), and hence lower the electrical field crowding at the drain-side of the gate edge. Physically, the effect is related to a depletion region expansion and should help reduce trapping effects and increase the breakdown voltages. Karmalkar *et al.*[20] showed through simulations that a FP over a stepped insulator is superior to an overlapping gate scheme, and that much higher breakdown voltages could be attained. In RF AlGaN/GaN HEMT devices, since the gate can still be a Schottky contact, the field plates will not compromise the transconductance significantly. Additionally, the use of high-k dielectric materials to cover the surface of the semiconductor device could boost the breakdown voltage.[21] Given the large difference in the permittivity between the high-k dielectrics and AlGaN, a high-k film can be expected to transmit electric flux into or extract electric flux from the semiconductor surface more efficiently. As a result, the peak field at the drain side edge of the gate electrode could be decreased. It may be mentioned in this context of high-k dielectrics that inorganic materials such as PZT [$Pb(Zr_{0.53}Ti_{0.47})O_3$] and Barium Strontium Titanate can have potential problems because of their hysteresis behavior which would seriously impact the high-frequency performance of HEMTs. However, high-k materials such as HfO_2 or Ta_2O_5, which are relatively hysteresis-free[22] are ideal candidates for the present application.

In this contribution, calculations of electric field distributions in GaN HEMTs based on physics-based models that include polarization effects are performed to gauge the potential for mitigating the internal device fields, and hence the Inverse Piezoelectric Effect. For completeness, the role of thermal heating is also analyzed. The possible mitigation of IPE degradation by reducing the internal electric fields (and hence the related elastic energy) by using a HfO_2 "cap layer" above the AlGaN barrier is also studied. Finally, simulations are performed to quantify even larger reductions in the internal electric fields by using "field plates". The results of using a separate gate-field-plate and a source-field-plate are also probed in this model analysis.

II. MODEL AND METHOD

Calculations of stress, strain and elastic energy density in the AlGaN barrier layer were modeled to quantify the role of the internal electric fields. The normal to the interface was taken to be along the z-direction, while the channel direction was along the x-axis. The equations for nomal stress (T_1), planar strain (S_{10}), vertical strain (S_3) and elastic energy density (W) are given as:[7]

$$S_{10} = (a_{GaN}\text{-}a_{AlGaN})/a_{AlGaN}, \tag{1a}$$

$$S_3 = -\frac{2C_{13}}{C_{33}}S_{10} + \left(\frac{e_{33}}{C_{33}}\right)E_z, \tag{1b}$$

$$T_1 = \left(C_{11} + C_{12} - \frac{2{C_{13}}^2}{C_{33}}\right)S_{10} + (\frac{C_{13}e_{33}}{C_{33}} - e_{31})E_z, \tag{1c}$$

$$W = \frac{C_{33}}{C_{11}C_{33} - 2{C_{13}}^2 + C_{12}C_{33}} * {T_1}^2, \tag{1d}$$

where E_z is the electric field in vertical (normal to interface) direction. A number of physical properties such as the dielectric constant $\varepsilon(x)$, the Schottky barrier height $q\varphi_b$(x), the conduction band offset $\Delta E_c(x)$ and band gap $E_g(x)$, the lattice constant $a(x)$, $P_{sp}(x)$ the spontaneous polarization, the piezoelectric coefficients $e_{13}(x)$, $e_{33}(x)$, and the elastic coefficients $C_{13}(x)$, $C_{33}(x)$ are functions of the mole fraction x of the Aluminum in the layer (i.e., in $Al_xGa_{1-x}N$). The following equations were used to connect the mole fraction x to these quantities:

$$\varepsilon(x) = \text{-}0.3x + 10.4, \tag{2a}$$

$$\varphi_b(x) = (1.3x + 0.84)\,eV, \tag{2b}$$

$$\Delta E_c(x) = 0.7|E_g(x) - E_g(0)|, \tag{2c}$$

$$E_g(x) = [6.13x + 3.42(1 - x) - x(1 - x)]\,eV, \tag{2d}$$

$$\varepsilon(x) = \text{-}0.3x + 10.4, \tag{2e}$$

$$C_{13}(x) = (5x + 103)\,GPa, \tag{2f}$$

$$C_{33}(x) = (\text{-}32x + 405)\,GPa, \tag{2g}$$

$$e_{ij}(x) = [e_{ij}(AlN) \text{-} e_{ij}(GaN)]x + e_{ij}(GaN), \tag{2h}$$

$$P_{SP}(x) = (\text{-}0.052x - 0.029)\,C/m^2, \tag{2i}$$

$$a(x) = (\text{-}0.077x + 3.189)\,\text{Å}, \tag{2j}$$

where the unstrained value of the lattice constant for GaN was taken to be 3.189 Å. Also, the piezoelectric coefficients for AlN and GaN were taken from the literature[23] and were set to: $e_{31} = \text{-}0.6$ and $e_{33} = 1.46$ for AlN, and e_{31} = -0.49 and e_{33} = 0.73 for GaN.

The sheet carrier concentration n_s at the AlGaN/GaN interface was calculated using the theory outlined by Ambacher et al,[22] and given by:

$$n_s(x) = \frac{\sigma(x)}{q} - (\frac{\epsilon_0\epsilon(x)}{dq^2})[q\varphi_b(x) + E_F(x) - \Delta E_c(x)], \tag{3a}$$

$$\text{where } \sigma(x) = \left|\frac{2(a(0) - a(x))}{a(x)}\left\{e_{31}(x) - \frac{e33(x)\,C13(x)}{C33(x)}\right\} + P_{sp}(x) - P_{sp}(0)\right|, \tag{3b}$$

$$E_F(x) = E_o(x) + (\pi\hbar^2/m^*(x)) * n_s(x), \tag{3c}$$

$$E_0(x) = \left\{ \frac{9\pi\hbar^2 q^2}{8\epsilon_0\epsilon\sqrt{8m^*(x)}} n_s(x) \right\}^{\frac{2}{3}}. \tag{3d}$$

In the above, d is the AlGaN layer thickness, σ represents polarization induced sheet charge density, E_F is the Fermi level with respect to GaN conduction band edge energy, and q is electron charge. In the above, the sheet charge is determined by the polarization consisting of both the piezoelectric and spontaneous polarization components.

The two-dimensional (2D) electrostatics for electric field and electric potential distributions across the HEMT device based on solutions of the Poisson equation was computed using the COMSOL Multiphysics software. A 2D triangular mesh with manual refinement was used with the maximum mesh element size set to 0.2 μm and the minimum size of 0.002 μm. This finite element COMSOL Multiphysics model was also been used to determine the stress/strain behavior, as well as internal device heating. The current flow in the channel leading to power dissipation represented the heat source. Boundary conditions used for the calculations were as follows: (i) Zero charge condition was used for all the exterior boundaries (i.e., $n.D$ =0 where D is electric displacement, and n the unit normal). (ii) Charge conservation [i.e., $n.(D_1\text{-}D_2)$=0] was used for interior boundaries with zero surface charge. (iii) For the OFF state, σ (representing the combined spontaneous and piezoelectric polarization charge densities) values were applied at the AlGaN/GaN interface and a negative charge density of $|n_s\, q|$ was applied at the top of the AlGaN layer between source-to-gate and gate-to-drain. (iv) Potentials V_G and V_D were set for the Gate and Drain contacts, respectively, with the source regions at zero potential. A gradual transition of voltage between the source-gate and gate-drain regions along the top AlGaN surface was used by applying a boundary condition which resulted in a linear transition of potential with location.

For completeness, temperature changes due to device operation were analyzed by the COMSOL tool, using its Heat Transfer module. The governing equation is, upon neglecting viscous heating and pressure-work terms:

$$\rho\, C_p \frac{\delta T}{\delta t} - \nabla \cdot (\mathrm{k}\nabla T) = Q - \rho\, C_p\, \boldsymbol{u} \cdot \nabla T, \tag{4a}$$

where k is the thermal conductivity (W $\mathrm{m}^{-1} \cdot \mathrm{K}^{-1}$), ρ is the mass density (kg m^{-1}), C_p is the specific heat capacity at constant pressure (J Kg^{-1} K^{-1}), T is the absolute temperature (K), Q the heat source term (W m^{-3}), and $\boldsymbol{u}$ the velocity vector. If both radiation and convection effects are excluded, equation (4a) simplifies to:

$$\rho\, C_p \frac{\delta T}{\delta t} - \nabla \cdot (\mathrm{k}\nabla T) = Q, \tag{4b}$$

The thermal boundary conditions were assigned as discussed in a model by Menozzi et al.[24]. The bottom substrate surface was maintained at a constant 300 K (i.e., isothermal room-temperature condition), while the top GaN surface and the remaining exterior model boundaries were considered adiabatic. The power dissipation value across the AlGaN/GaN interface was taken to be $E\,J$ ($\mathrm{W/m}^2$), with E being the electric field values at the interface and J the channel current density. The later was calculated as $n_s\, q\, \upsilon$ with υ being is the field-dependent electron drift velocity. The following description was used for the drift velocity:[25]

$$\upsilon(x) = \frac{\left\{ \mu_0 E\,(x) + \upsilon_s * \left[\frac{E(x)}{E_1} \right]^5 \right\}}{\left\{ 1 + \left[\frac{E(x)}{E_0} \right]^5 \right\}}, \tag{5}$$

where $\upsilon(x)$ represents the drift velocity as a function of position, υ_s is the saturation velocity (taken to be 2.1x10^7 cm/s), μ_0 = 260 cm^2/V s denotes the electron mobility, E_0 = 15.9x10^4 V/cm, and E_1 = 17.2x10^4 V/cm. The complete set of parameters used in this modeling is given in Table I.

TABLE I. Parameters used for the AlGaN-GaN HEMT simulations.[7]

Parameter	Value
x (Al fraction)	0.26, 0.28, 0.3
a (lattice constant)	$3.189e^{-10}$ (GaN), $3.112e^{-10}$ (GaN),
ε_r (dielectric constant)	9.5 (GaN), 9.0 (AlN)
$\hbar$ (Plancks constant)	$6.5x10^{-16}$ eVs
m^* (Effective mass)	$0.22x10^{-31}$ Kg
e_{31} (piezoelectric constant)	-0.49C/m^2 (GaN), -0.6C/m^2 (AlN)
e_{33} (piezoelectric constant)	0.73 C/m^2 (GaN), 1.46 C/m^2 (AlN)
C_{33} (elastic constant)	405 Gpa (GaN), 373 Gpa (AlN)
C_{11} (elastic constant)	350 GPa
C_{12} (elastic constant)	110 GPa
C_{13} (elastic constant)	103Gpa (GaN), 108 Gpa (AlN)
ρ (Density)	6095 (GaN), 3965 (Substrate) kg/m^3
K (Thermal Conductivity)	160 (GaN), 49 (substrate) W/ m K
C_p (Heat capacity at constant pressure)	410 (GaN), 730 (Substrate) J/ kg K
α_a (In-Plane thermal expansion coefficient)	48 x 10^{-7} (GaN) K^{-1}
α_c (Out of Plane thermal expansion coefficient)	43 x 10^{-7} (GaN) K^{-1}

III. SIMULATION RESULTS AND DISCUSSION

Simulations were first performed for the internal electric fields and elastic energy densities within HEMT structures subjected to various gate and drain biasing values. For verification and validation, device dimensions were chosen to be in keeping with the report by Joh et al.[7] Figures 1(a) and 1(b) show the vertical electric field and elastic energy profiles under the gate edge as obtained from our simulations. The energy density is shown at a y-position of 5.414 μm. The drain was chosen to be at 33V, the source was grounded, while the gate was at -5 V. These results match the vertical electric field and elastic energy profiles as reported by Joh et al.[7] for exactly the same drain and gate bias values. It can be seen that both the electric field values and elastic energy density values exhibit sharp peaks at the gate edge near the drain side, while the elastic energy density under the gate edge is at about 0.49 J/m^2. This location under the gate near the drain side is thus a potential weak spot for failure.

The effect of using a high-k dielectric material as a cap layer on AlGaN on the electric field distribution and the peak values was studied next. Both HfO_2 and Ta_2O_5 were used for the high-k dielectrics, and the results were similar. Hence, for clarity only results with a HfO_2 cap layer are presented and discussed here. Figure 2 shows the electric field profile for a HEMT with a 12 nm thick high-k cap layer. The gate length was taken to be 0.25 μm, the drain and source lengths were 0.5 μm each, the source-to-drain distance was taken to be 4 μm, while the AlGaN thickness was 16 nm. For a detailed analyses, four different structures were compared: (a) A simple AlGaN-GaN HEMT without any cap layer, (b) An AlGaN-GaN HEMT with a uniform 12 nm HfO_2 cap, (c) An AlGaN-GaN HEMT with a HfO_2 cap layer, but with a slight "notch" over a length of 0.5 μm (with a reduced HfO_2 thickness due to the notch over this distance) starting from the gate edge to its right, and (d) An AlGaN-GaN HEMT with a HfO_2 cap layer, but with a slight "mesa" of length 0.5 μm (with the HfO_2 thickness increased by 12 nm across the mesa) just to the right of the gate as shown in Fig. 3. Simulation results obtained for the electric field distribution in the AlGaN layer at a 5.413 micron vertical distance for the four different configurations are shown in Fig. 4. Two main results emerge from the plots of Fig. 4. First, the addition of a high-k cap layer does work to reduce the peak electric fields. For example, the highest and sharpest peaks are predicted for the simple AlGaN-GaN HEMT without any cap layer. The addition of a uniform high-k layer does reduce the electric field from about 9.5 MV/cm to roughly 7 MV/cm. Furthermore, in the presence of a 0.5 micron long, 12 nm deep notch in the high-k HfO_2 layer, the electric field is slightly increased as compared to the case of the uniform high-k cap. Furthermore, the inclusion of a 0.5 micron long, 12 nm thick high-k mesa structure on top of the cap layer, shows the sharpest reduction. The electric

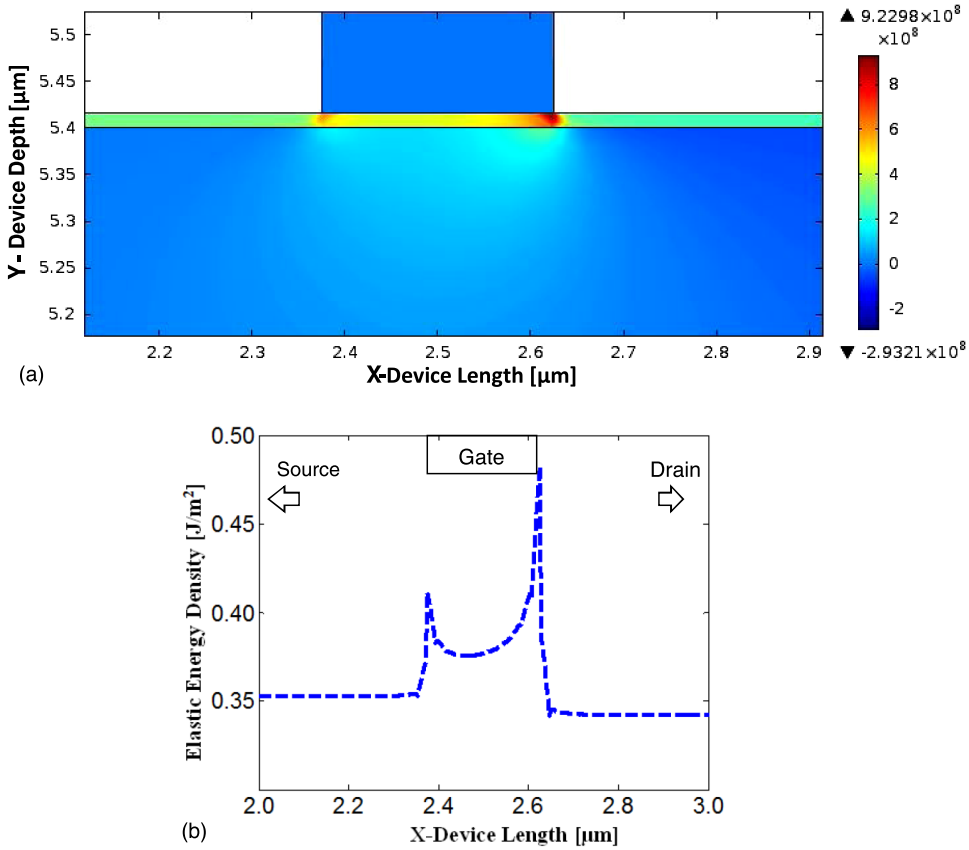

FIG. 1. Simulation results for a GaN-AlGaN HEMT. (a) Vertical electric field profile with V_d=33V and Vg=-5V. (b). Corresponding elastic energy density in the AlGaN layer at 5.414 µm.

field peak is seen to be lowered down to 5.75 MV/cm in Fig. 4. Thus, the results clearly show the advantage of using high-*k* materials in the context of the HEMT device. Furthermore, by tailoring the geometry and structure of the high-*k* layer, further improvements could be achieved. For example, the height of the mesa structure as well as its length could be changed, and a step-profile could be added to further modulate and suppress the electric fields.

Another improvement towards the mitigation of the high electric fields at the gate (near the drain side) was obtained by the use of "field plates." The structure used in the simulations and

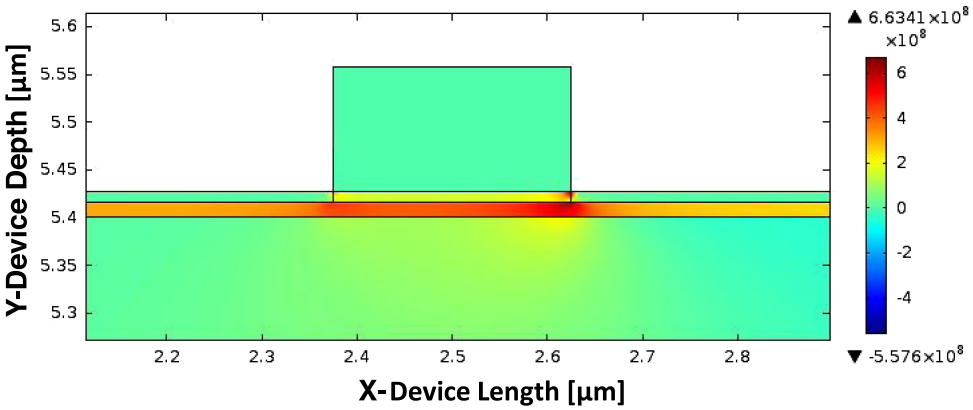

FIG. 2. Electric field profile in AlGaN/GaN HEMT with high-*k* cap layer.

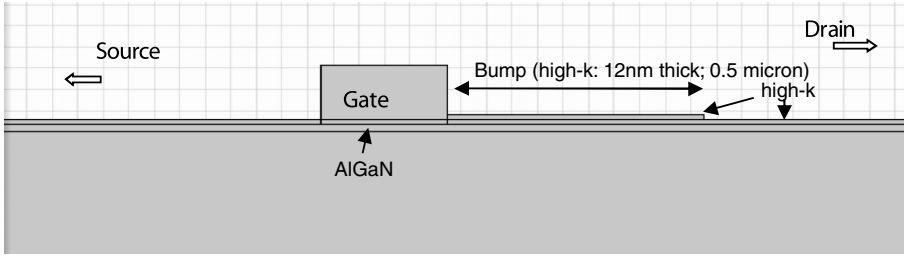

FIG. 3. HEMT structure having a high-k layer with an additional 0.5 μm mesa just to the right of the gate.

the results for the electric field distribution with a *gate field plate* are shown in Figs. 5 and 6, respectively. The dimensions of the electrodes, AlGaN thickness and the source-drain distance were all kept at the same values as discussed in the context of Fig. 2. The thickness of field plate used was 12 nm. The peak electric field in Fig. 6 is seen to be about 4 MV/cm which is significantly less than the peak value in Fig. 4 without the gate plate. For completeness, simulations were also carried out for the same structure but with a source field plate. The electric field distribution with a *source field plate* is shown in Fig. 7. In this case, the peak electric field is about 5.3 MV/cm, but still substantially lower than the previous results of Fig. 4 without any field plates. However, the values of Fig. 7 are somewhat higher than those obtained with the gate field plate shown in Fig. 6. Hence, the use of a gate field plate in concert with a high-k oxide would seem to be the best configuration for HEMTs for mitigating device degradation. It may be mentioned for completeness that though the gate field plates show the most significant improvement in breakdown fields, this would come at the cost of additional parasitic capacitance. Such a capacitance increase could have the adverse effect of reducing current gain and the power gain at the cut-off frequency. This would occur because in the gate field configuration, the capacitance between the FP and drain contributes to the gate-to-drain capacitance (C_{gd}), resulting in negative Miller feedback. This could cause reduction in current-gain and power-gain cutoff frequencies.

The impact and advantage of having the high-k HfO_2 dielectric and the mesa structure in mitigating potential IPE within the HEMT devices can be better assessed through an evaluation of the internal elastic energy density profile. As has been reported previously,[7] if the internal elastic energy exceeds a critical value of about 0.49 J/m^2, then crystallographic defects can begin to formed that are electrically active. This defect formation can provide a path for excess gate leakage current, and

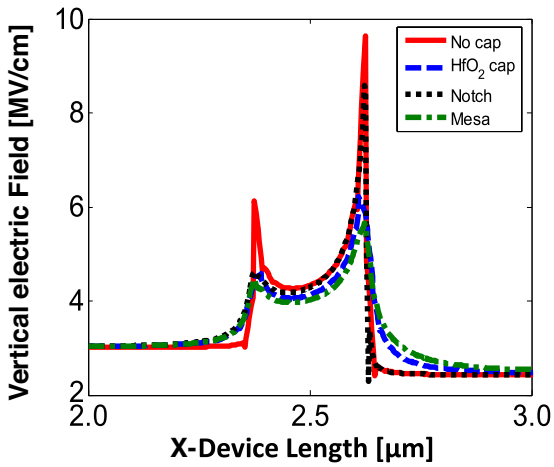

FIG. 4. Electric field distribution in the AlGaN layer at a 5.413 micron vertical height for 4 different configurations. These were without any cap layer, a uniform HfO_2 cap layer on top of the AlGaN material, a 0.5 micron long, 12 nm deep notch in the high-k HfO_2 layer, and a 0.5 micron long, 12 nm raised high-k mesa over the first 0.5 microns of the HfO_2 cap layer near the gate edge.

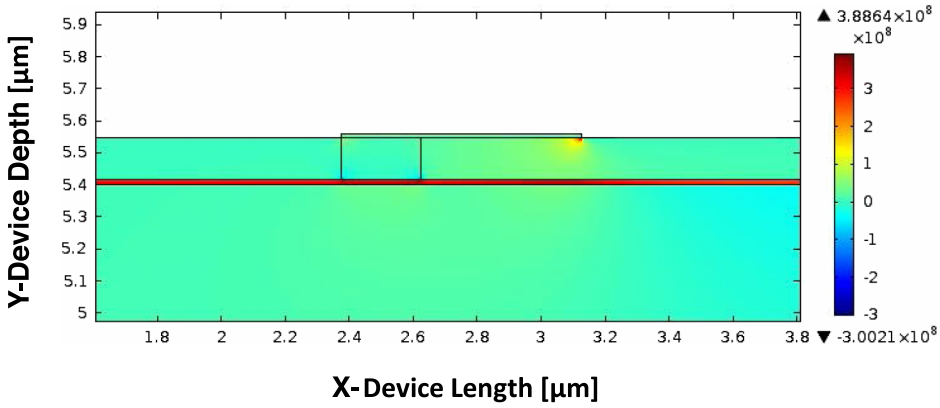

FIG. 5. Simulated structure for the GaN-AlGaN-Gate Field Plate with HfO_2 layer.

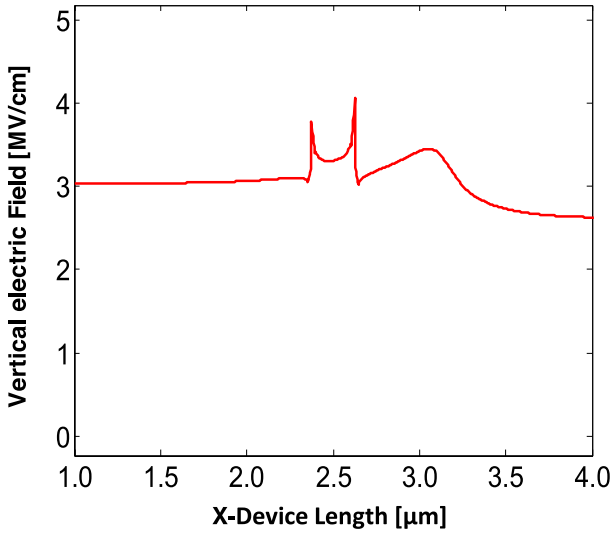

FIG. 6. Electric field in AlGaN layer at a vertical (y) position of 5.414 µm.

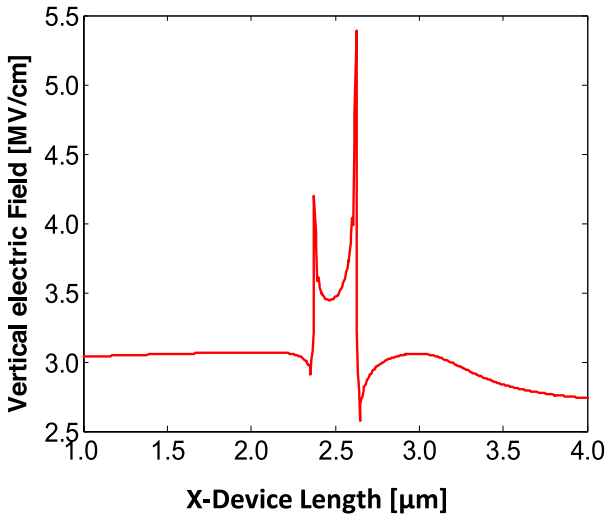

FIG. 7. Electric field in AlGaN layer at a vertical (y) position of 5.414 µm with source field plate.

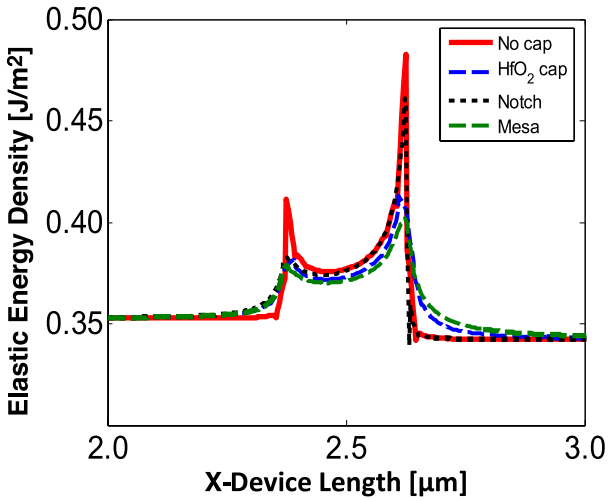

FIG. 8. Calculated results showing the energy density profile at 5.405 micron vertical height for five different structures of an AlGaN/GaN HEMT. The lowest energy density values are with the mesa structure with a high-k layer.

result in electron trapping that depletes the sheet charge in the channel resulting in device degradation. Hence, a convenient measure of device stability with regards to potential inverse piezoelectric effects is based on the maximum value of the internal energy density. Structures that reduce this stored energy density and yield profiles that are substantially below the 0.49 J/m^2 threshold would naturally promote stability and be preferred. Figure 8 shows the energy density profile at 5.405 micron vertical height for five different structures of an AlGaN/GaN HEMT. The five different configurations chosen were: (i) AlGaN without a capping layer, (ii) AlGaN with a uniform high-k HfO_2 cap layer, (iii) A 12 nm thick, 0.5 micron-long notch in the high-k HfO_2 layer with fixed negative charge on AlGaN surface except under the gate region, (iv) A 22 nm thick,0.5 micron-long notch in high-k HfO_2 cap layer with fixed negative charge on AlGaN surface except under gate region, and (v) A 0.5 micron wide and 12 nm thick high-k elevated mesa layer near the gate edge above a high-k cap layer. As seen from the figure, the lowest energy density values are with the mesa structure on a high-k layer. Thus, this configuration is predicted from the energy standpoint to provide the most robust structure with respect to potential deleterious inverse piezoelectric effects.

For completeness, the issue of device heating was studied to probe the potential for temperature driven defect formation. The point was simply to test the hypothesis that the IPE is more significant than increases in stress due to thermal heating. Figure 9 shows the power density calculated across the AlGaN/GaN interface with the Aluminum mole fraction taken to be 0.28, an AlGaN thickness (t_{AlGaN}) of 16nm, and a 20 V drain bias. The temperature distribution due to these power density values is shown in Fig. 10 for a 300K ambient temperature. The predicted temperature increase is about 3K, and hence very insignificant. Thus, these results underscore the irrelevance of thermal heating and suggest that temperature increases would not play any significant role in contributing to internal stresses or degradation of GaN HEMT structures.

A final comment concerns the possible negative effects of the FP on the frequency response. In this regard, the cutoff frequency f_T is influenced by either the unity current gain,[26] or dictated by the transit time The latter involves the saturation velocity v_s, the drain-to-gate length L_{dg}, the source-to-gate length L_{sg} and the gate channel length L_c, with the transit time τ_{tr} being roughly given as: $\tau_{tr} = v_s/[L_{sg} + L_c + L_{dg}]$. The unity current gain equals $g_m/[2\pi C_g]$, where g_m is the transconductance and C_g the gate capacitance. Since the FP is practically an extension of the gate, it may be expected to have a geometric influence on the gate capacitance. For example, very roughly, the contribution of the field plate to the capacitance, C_{FP}, would simply add to the gate capacitance C_g. Furthermore, the transconductance g_m roughly reduces with the channel length,[27] making the cut-off frequency f_T decrease with the field plate roughly by a $[1 + C_{FP}/C_g]^{-2}$ factor As a result, the field

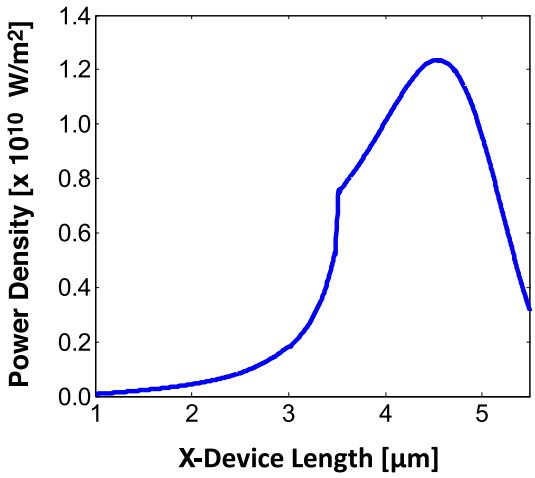

FIG. 9. Calculated power density variation across the AlGaN/GaN interface.

plate lengths should be kept relatively modest to minimize this trade-off with the device frequency response.

For completeness, it may be mentioned that in practice, the dependence on the gate length can be far more complicated. For example, most scaling rules used are often based on simple notions such as the gradual channel approximation and constant mobility. However, non-equilibrium carrier dynamics (including ballistic transport) can lead to drift velocity behavior that is dominated by velocity overshoot, in the case of short gate lengths that are on the order of the electronic inelastic mean free paths. Under such situations, the transconductance can increase with reductions in gate length.[28] Basically, at relatively larger values of the gate lengths, the response is dominated by the gate-fringing effect. This gate-fringing is induced by a non-planar depletion layer under the gate, with the capacitance acting less like a parallel plate capacitor and more like a circular capacitor. However, once the gate length reduces further and becomes on the order of the inelastic mean

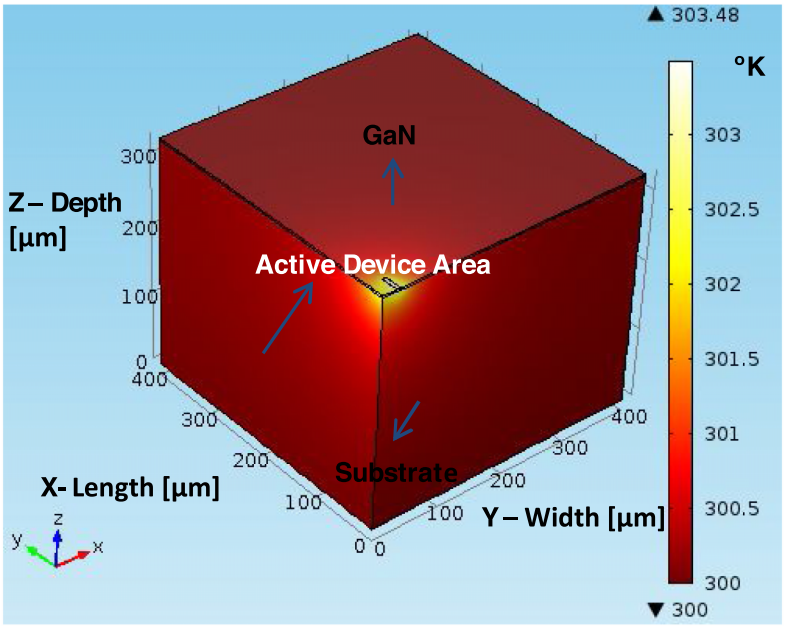

FIG. 10. Temperature distribution across GaN/Substrate from a thermal 3D model.

free path of electrons, then velocity over-shoot starts to occur and dominates the response over the gate-fringing effect. In the present situation, since the use of high-k dielectric layer would naturally reduce the electric fields,[29] the use of a long field plate to shape the potential distribution would not be necessary. As a final comment, optimized field-plate engineering could be a potential next step for optimizing HEMT devices,[30] but is beyond the present scope.

IV. CONCLUSIONS

Calculations of electric field and potential distributions across GaN HEMTs were carried out based on physics-based models to probe the role of internal electric fields on IPE-based degradation and their possible mitigation. The focus was also on the possible mitigation of the IPE degradation by reducing the internal electric fields and related elastic energy through the use of high-k materials. The contributions to possible device failure based on both the Inverse Piezoelectric Effect (IPE) as well as the Thermal heating were analyzed. Basic results for a simple situation compared well with a published report. The simulations also showed the thermal effects to be negligible, and that the main danger for device degradation would be the IPE, especially during the OFF-state of HEMT devices. Use of a HfO_2 "cap layer" above the AlGaN barrier was shown to reduce the electric fields. In particular, the use of a mesa structure was shown to be especially effective. Simulations were also performed to fashion even larger reductions in the internal electric fields by using "field plates" in concert with a high-k layer The use of a gate plate with a HfO_2 cap layer appears to be a very useful strategy for mitigating device degradation and failures.

ACKNOWLEDGMENTS

The work was supported by a grant from US Army Research Office (CEAND, W911NF-11-1-0209). The authors would like to acknowledge Hao Qiu (ODU) for help on some calculations, and gratefully appreciate discussions with Prof. U. Mishra (UCSB).

[1] U. K. Mishra, P. Parikh, and Y.-F Wu, Proceedings of the IEEE **90**, 1022 (2002).
[2] E. Zanoni, M. Meneghini, A. Chini, D. Marcon, and G. Meneghesso, IEEE Transactions on Electron Devices **60**, 3119 (2013).
[3] U. K. Mishra, L. Shen, T. E. Kazior, and Y-F. Wu, Proceedings of the IEEE **96**, 287 (2007).
[4] T. Kikkawa, K. Makiyama, T. Ohki, M. Kanamura, K. Imanishi, N. Hara, and K. Joshin, Physica Status Solidi A **206**, 1135 (2009).
[5] B. J. Baliga, IEEE Trans. Electron Devices **43**, 1717 (1996).
[6] A. A. Villanueva, J. A. del Alamo, T. Hisaka, K. Hayashi, and M. Somerville, IEEE Transactions on Device and Materials Reliability **8**, 283 (2008).
[7] J. Joh, F. Gao, T. Palacios, and J. A. del Alamo, Microelectronics Reliability **50**, 767 (2010).
[8] J. A. del Alamo and J. Joh, Microelectronics Reliability **49**, 1200 (2009).
[9] M. Faqir, G. Verzellesi, A. Chini, F. Fantini, F. Danesin, G. Meneghesso, E. Zanoni, and C. Dua, IEEE Transactions on Device and Materials Reliability **8**, 240 (2008).
[10] C. Nguyen, N. X. Nguyen, and D. E. Grider, Electron Lett **35**, 1380 (1999).
[11] M. A. Khan, M. S. Shur, Q. C Chen, and J. N. Kuznia, Electron. Lett. **30**, 2175 (1994).
[12] R. Vetury, N. Q. Zhang, S. Keller, and U. K. Mishra, IEEE Transactions on Electron Devices **48**, 1 (2001).
[13] Y.-F Wu, B. P. Keller, S. Keller, J. J. Xu, B. J. Thibeault, S. P. Denbaars, and U. K. Mishra, IEICE Transactions on Electronics **E-82**, 1895 (1999).
[14] S. C. Binari, K. Ikossi, J. A. Roussos, W. Kruppa, D. Park, H. B. Dietrich, D. D. Koleske, A. E. Wickenden, and R. L. Henry, IEEE Transactions On Electron Devices **48**, 465 (2001).
[15] C. Binary, K. Ikossi, J. A. Roussos, W. Kruppa, D. Park, H. B. Dietrich, D. D. Koleske, A. E. Wickenden, and R. L. Henry, IEEE Trans. Electron Devices **48**, 465 (2001).
[16] A. Koudymov, M. S. Shur, G. Simin, and R. Gaska, Phys. Statist. Solid **1**, 116 (2007).
[17] K. J. Choi and J. L. Lee, Appl. Phys. Lett. **75**, 1580 (1999).
[18] S. Karmalkar and U. K. Mishra, IEEE Electron Device Lett **48**, 1515 (2001).
[19] F. Conti and M. Conti, Solid State Electron. **15**, 93 (1972).
[20] S. Karmalkar and U. K. Mishra, Solid State Electron. **45**, 1645 (2001).
[21] F. T. Chu, C. Chen, W. Zhou, and X. Z. Liu, Chin. Phys. Lett **30**, 097303/ (2013) 1-4.
[22] J. Shen, C. Y. Zhang, T. T. Xu, A. N. Jiang, Z. Y. Zhang, S. Wang, and Q. Chen, Thin Solid Films **519**, 7723 (2011).
[23] O. Ambacher, J. Smart, J. R. Shealy, N. G. Weiman, K. Chu, M. Murphy, W. J. Schaff, L. F. Eastman, R. Dimitrov, L. Wittmer, M. Stuzmann, W. Rieger, and J. Hilsenbeck, Journal of Applied Physics **85**, 3222 (1999).

[24] R. Menozzi, G. A. Umana-Membreno, B. D. Nener, G. Parish, L. F. Sozzi, and U. K. Mishra, IEEE Transactions on Device and Materials Reliability **8**, 255 (2008).
[25] M. Moradi and P. Valizadeh, Journal of Applied Physics **109**, 1 (2011).
[26] S. Karmalkar and U. Mishra, Solid State Electronics **45**, 1645 (2001).
[27] D. Liu, M. Hudait, Y Lin, H. Kim, S. A. Ringel, and W. Lu, Solid State Electronics **51**, 838 (2007).
[28] J. Han and D. K. Ferry, Solid State Electronics **43**, 335 (1999).
[29] C. B. Goud and K. N. Bhat, IEEE Transactions on Electron Devices **41**, 1856 (1994).
[30] S. Karmalkar, M. S. Shur, G. Simin, and M. A. Khan, IEEE Transactions On Electron Devices **52**, 2534 (2005).